


Cite this: *RSC Adv.*, 2023, 13, 6861

Optical band gaps and spectroscopy properties of $\text{Bi}^{m+}/\text{Eu}^{n+}/\text{Yb}^{3+}$ co-doped ($m = 0, 2, 3$; and $n = 2, 3$) zinc calcium silicate glasses†

Ho Kim Dan,^{ab} Nguyen Dinh Trung,^{cd} Nguyen Minh Tam,^e L. T. Ha,^f
C. V. Ha,^g Dacheng Zhou^h and Jianbei Qiu^h

In this study, the indirect/direct optical band gaps and spectroscopy properties of $\text{Bi}^{m+}/\text{Eu}^{n+}/\text{Yb}^{3+}$ co-doped ($m = 0, 2, 3$; and $n = 2, 3$) zinc calcium silicate glasses under different excitation wavelengths were investigated. Zinc calcium silicate glasses with the main compositions of $\text{SiO}_2\text{--ZnO--CaF}_2\text{--LaF}_3\text{--TiO}_2$ were prepared by the conventional melting method. EDS analysis was performed to determine the elemental composition existing in the zinc calcium silicate glasses. Visible (VIS)-, upconversion (UC)-, and near-infrared (NIR)-emission spectra of $\text{Bi}^{m+}/\text{Eu}^{n+}/\text{Yb}^{3+}$ co-doped glasses were also investigated. Indirect optical band gaps and direct optical band gaps of Bi^{m+} -, Eu^{n+} - single-doped, and $\text{Bi}^{m+}\text{--Eu}^{n+}$ co-doped $\text{SiO}_2\text{--ZnO--CaF}_2\text{--LaF}_3\text{--TiO}_2\text{--Bi}_2\text{O}_3\text{--EuF}_3\text{--YbF}_3$ zinc calcium silicate glasses were calculated and analyzed. CIE 1931(x, y) color coordinates for VIS and UC emission spectra of $\text{Bi}^{m+}/\text{Eu}^{n+}/\text{Yb}^{3+}$ co-doped glasses were determined. Besides, the mechanism of VIS-, UC-, NIR-emissions, and energy transfer (ET) processes between Bi^{m+} and Eu^{n+} ions were also proposed and discussed.

Received 18th November 2022

Accepted 2nd February 2023

DOI: 10.1039/d2ra07310b

rsc.li/rsc-advances

1. Introduction

During the last several decades, the optical band gaps and spectroscopy properties of host materials single-doped by a rare earth (RE) atom as well as co-doped by rare earth ions (REIs), or doped by REIs together with transition metals (TMs)^{1,2} or pnictogen³ have been extensively studied due to their great potential for applications in many technological fields such as displays, solar cells, and medical diagnosis.^{4–6} Among the REIs, europium ions (Eu^{n+}) have attracted much research interest, particularly in lighting, light emitting diodes (LED), white LED (WLED), and display applications owing to

the Eu^{n+} ions favoring existing in two valence states as the Eu^{3+} trication and Eu^{2+} dication in glass materials with $^5\text{D}_0 \rightarrow ^7\text{F}_j$ ($j=0, 1, 2, 3$, and 4) and $4\text{f}^65\text{d}^1 \rightarrow 4\text{f}^7$ transitions, respectively.^{7,8} Visible (VIS) emission spectra of $\text{Eu}^{3+}/\text{Eu}^{2+}$ ions can emit blue, green, orange, orange-red, and red color light depending on the different excitation wavelengths and host materials.^{9,10} Bismuth (Bi) element is the post-transition metal belonging to the pnictogen group; Bi exhibits many optoelectronic properties and exists in various valence states such as Bi^{5+} , Bi^{3+} , Bi^{2+} , Bi^+ , and Bi^0 depending on the experimental conditions and the host materials. In the VIS wavelength region, the $^1\text{P}_1 \rightarrow ^1\text{S}_0$ transition of Bi^{3+} ions can emit blue color light,^{11,12} and the $^2\text{S}_{1/2}$ -, $^2\text{P}_{3/2}(2)$ -, $^2\text{P}_{3/2}(1)$ - \rightarrow $^2\text{P}_{1/2}$ transitions of Bi^{2+} ions can emit orange, orange-red, and red color light, respectively.^{12,13} In the near-infrared (NIR) wavelength region, the $^3\text{P}_2$ -, $^3\text{P}_1$ - \rightarrow $^3\text{P}_0$ transitions of Bi^+ ions and the $^2\text{D}_{3/2}$ - \rightarrow $^4\text{S}_{3/2}$ transition of Bi^0 neutral can produce NIR emission bands from ~ 1.0 to $1.35 \mu\text{m}$.^{14,15} In addition, Bi^{m+} ($m = 0, 2$, and 3) ions can combine with the $^2\text{F}_{5/2} \rightarrow ^2\text{F}_{7/2}$ transition of Yb^{3+} ions to generate NIR emission spectra in the ~ 950 nm to 1350 nm wavelength region.^{16,17} Therefore, NIR emission spectra of $\text{Bi}^{m+}\text{--Yb}^{3+}$ have been extensively studied with the aim of improving the efficiency and quantum effect of NIR emission spectra utilized in solar cell applications.^{18,19} In recent years, many investigations focusing on the energy transfer (ET) processes from Bi^{m+} to Eu^{3+} ions that can be color-tuned in the VIS emission to create light bands with different colors have been carried out. The obtained results

^aOptical Materials Research Group, Science and Technology Advanced Institute, Van Lang University, Ho Chi Minh City, Vietnam

^bFaculty of Applied Technology, School of Technology, Van Lang University, Ho Chi Minh City, Vietnam. E-mail: hokimdan@vlu.edu.vn

^cCenter for Analysis and Testing, Dalat University, Lam Dong, Vietnam

^dFaculty of Chemistry and Environment, Dalat University, Lam Dong, Vietnam

^eFaculty of Basic Sciences, University of Phan Thiet, 225 Nguyen Thong, Phan Thiet City, Binh Thuan, Vietnam

^fInstitute of Science and Technology, TNU-University of Sciences, Thai Nguyen, 250000, Vietnam

^gFaculty of Physics, TNU-University of Education, Thai Nguyen, 250000, Vietnam

^hKey Laboratory of Advanced Materials of Yunnan Province, School of Materials Science and Engineering, Kunming University of Science and Technology, Kunming 650093, China

† Electronic supplementary information (ESI) available. See DOI: <https://doi.org/10.1039/d2ra07310b>


confirmed that the energy was transferred from Bi^{3+} and Bi^{2+} ions to $^5\text{D}_0 \rightarrow ^7\text{F}_j$ ($j=0, 1, 2, 3$, and 4) transitions of Eu^{3+} and thus color-tuned the VIS emission spectra of $\text{Eu}^{3+}/\text{Eu}^{2+}$ ions.^{20–23} Besides, the measurement and calculation of the optical band gap parameters of REIs doped in different host materials have also been performed to determine the optical band gap energy (E_g) value of REIs in the host materials²⁴ and thereby directing the relevant optical applications such as color display, LED, WLED, and solar energy. Zinc silicate glasses can be used for optical material applications due to their advantages such as high thermal expansion properties,²⁶ relatively low glass transition temperature (T_g), and the value of $\Delta T = T_c - T_g$ greater than 100.²⁵ Based on these advantages as well as the results obtained from a recent study,²⁵ in this work, we chose zinc calcium silicate glass as the host material. In addition, Na_2O was replaced by CaF_2 to enhance the self-reduction process from Eu^{3+} to Eu^{2+} ions through F^- ions.⁸ Simultaneously, we investigated and reported the results concerning the direct/indirect optical band gaps, VIS-, UC-, and NIR-emission spectra of $\text{Bi}^{m+}/\text{Eu}^{n+}/\text{Yb}^{3+}$ co-doped in SiO_2 - ZnO - CaF_2 - LaF_3 - TiO_2 (SZC) zinc calcium silicate glasses. Remarkably, through analyzing the optical properties of $\text{Bi}^{m+}/\text{Eu}^{n+}/\text{Yb}^{3+}$ co-doped, we have also calculated and determined the direct/indirect optical band gaps values, CIE 1931 (x, y) color coordinates to develop for LED, WLED, and display applications.

2. Experimental materials and methods

2.1. Materials

Raw materials of SiO_2 , ZnO , CaF_2 , LaF_3 , TiO_2 , Bi_2O_3 , EuF_3 , and YbF_3 used in the experiments of this study are high-purity laboratory-grade materials (99.99%). Chemical compositions and ratios for each glass sample are listed in detail in Table 1.

2.2. Experimental methods

The raw material mixtures weighing 12 g for each experimental glass sample were crushed with an onyx mortar and pestle.^{8,27} These mixtures were compacted into platinum crucibles with lids.⁸ The platinum crucibles with lids were then placed in an electric furnace to melt at 1600 °C for 1 hour using the conventional melting method.^{8,27} After melting, the mixture was quenched on the surface of the polished stainless steel plate to form the glass.⁸ Glass samples were heat treated at 520 °C for 6 hours^{8,25} to increase mechanical strength and reduce the possibility of breakage when cut. For the convenience and accuracy of optical measurements, glass samples were cut to the size of 10 mm × 10 mm × 2 mm with polished surfaces and edges.⁸ Details for EDS analysis, absorption spectra, VIS-, UC-, and NIR-emission spectra measuring and analyzing devices have been described in detail in our recent studies.^{8,27–29}

3. Results and discussion

3.1. EDS analysis

Fig. 1 shows the results of the EDS spectrum analysis of the SZC-1.0Bi0.6Eu2Yb zinc calcium silicate glass sample. Energy levels at ~0.45 and 4.51 keV were determined for titanium (Ti) element,³⁰ energy levels at ~2.42 and 10.84 keV were determined for the Bi element, energy levels at ~0.83 and 4.65 keV were attributed to lanthanum (La) element.³⁰ Energy levels of the Eu element were defined at ~1.13 and 5.85 keV.³⁰ Energy levels of the ytterbium (Yb) element were also defined at ~1.52 and 7.41 keV. Energy levels at ~0.53, 0.68, 1.74, 3.69, and 8.63 keV were determined for oxygen (O), fluorine (F), silicon (Si), calcium (Ca), and zinc (Zn) elements, respectively.^{30,31} The element composition table including weight and atomic percentages of the SZC-1Bi0.6Eu2Yb zinc calcium silicate glass sample inserted in Fig. 1 also described in detail the

Table 1 Chemical compositions and ratios of SiO_2 - ZnO - CaF_2 - LaF_3 - TiO_2 - Bi_2O_3 - EuF_3 - YbF_3 glasses

Notation of glass samples	Chemical compositions and ratios of glasses (in mol%)							
	SiO_2	ZnO	CaF_2	LaF_3	TiO_2	Bi_2O_3	EuF_3	YbF_3
SZC-1Bi	45	25	15	10	4	1.0	0	0
SZC-0.6Eu	45	25	15	9.4	5	0	0.6	0
SZC-1Bi0.6Eu	45	25	15	9.4	4	1.0	0.6	0
SZC-1.8Bi0.6Eu	45	25	15	9.4	3.2	1.8	0.6	0
SZC-1.0Bi0.6Eu2Yb	45	25	15	7.4	4	1.0	0.6	2.0
SZC-1.2Bi0.6Eu2Yb	45	25	15	7.4	3.8	1.2	0.6	2.0
SZC-1.4Bi0.6Eu2Yb	45	25	15	7.4	3.6	1.4	0.6	2.0
SZC-1.6Bi0.6Eu2Yb	45	25	15	7.4	3.4	1.6	0.6	2.0
SZC-1.8Bi0.6Eu2Yb	45	25	15	7.4	3.2	1.8	0.6	2.0
SZC-1.8Bi0.7Eu2Yb	45	25	15	7.3	3.2	1.8	0.7	2.0
SZC-1.8Bi0.8Eu2Yb	45	25	15	7.2	3.2	1.8	0.8	2.0
SZC-1.8Bi0.9Eu2Yb	45	25	15	7.1	3.2	1.8	0.9	2.0
SZC-1.8Bi1.0Eu2Yb	45	25	15	7	3.2	1.8	1.0	2.0
SZC-1.8Bi0.6Eu2.2Yb	45	25	15	6.8	3.2	1.8	0.6	2.2
SZC-1.8Bi0.6Eu2.4Yb	45	25	15	6.6	3.2	1.8	0.6	2.4
SZC-1.8Bi0.6Eu2.6Yb	45	25	15	6.4	3.2	1.8	0.6	2.6
SZC-1.8Bi0.6Eu2.8Yb	45	25	15	6.2	3.2	1.8	0.6	2.8



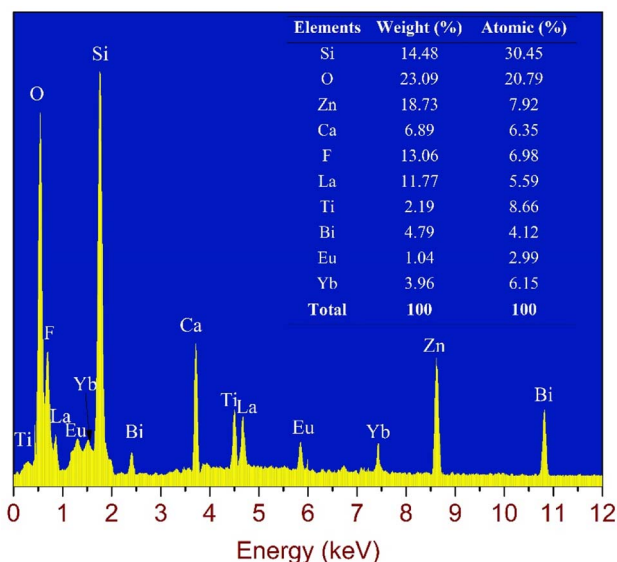


Fig. 1 EDS spectrum of SZC-1.0Bi0.6Eu2Yb zinc calcium silicate glass sample.

proportions of elements present in the host glass. From the results of the EDS analysis, it can be seen that all elements Si, O, Zn, Ca, F, La, Ti, Bi, Eu, and Yb presenting in $\text{SiO}_2\text{-ZnO-CaF}_2\text{-LaF}_3\text{-TiO}_2\text{-Bi}_2\text{O}_3\text{-EuF}_3\text{-YbF}_3$ raw materials were distributed and existed in zinc calcium silicate glass matrix.

3.2. Absorption spectra

Absorption spectra of SZC-1.0Bi, SZC-0.6Eu, and SZC-1.0Bi0.6Eu zinc calcium silicate glass samples in the wavelength range from 300 to 1200 nm are shown in Fig. 2. Curve (a) (black curve) in Fig. 2 is the absorption spectrum of Bi^{m+} ions which has three main bands, generated by the transitions of Bi^{m+} ions, with the peaks at ~ 458 , 653, and 700 nm, corresponding to $^1\text{S}_0 \rightarrow ^3\text{P}_1$ transition of Bi^{3+} ions,^{11,18,29} $^4\text{S}_{3/2} \rightarrow ^2\text{P}_{1/2}$ transition of Bi^{0+}

ions,^{14,15} and $^2\text{P}_{1/2} \rightarrow ^2\text{P}_{3/2}(1)$ transition of Bi^{2+} ions.¹³ We did not analyze and discuss the absorption spectrum of Bi^{m+} ($m = 0, 2$, and 3) ions in detail in this study. The absorption spectrum of the SZC-0.6Eu zinc calcium silicate glass sample is shown by curve (b) (red curve) in Fig. 2. It can be observed that the absorption spectrum of this curve includes four main absorption peaks at ~ 394 , 434, 465, and 536 nm corresponding to transitions from $^7\text{F}_0$ ground-state to $^5\text{L}_6$, $^5\text{D}_3$, $^5\text{D}_2$, and $^5\text{D}_1$ excited states of Eu^{3+} ions.^{7,8,32} The absorption spectrum of the SZC-1.0Bi0.6Eu zinc calcium silicate glass sample is shown by curve (c) (blue curve) of Fig. 2. This absorption spectrum includes all the absorption peaks of Bi^{m+} and Eu^{n+} ions present in curves (a) and (b) due to overlapping and combining absorption spectra of Bi^{m+} and Eu^{n+} ions.^{7,8,11,13,32} The images inserted in Fig. 2 are photographs of SZC-1Bi, SZC-0.6Eu, and SZC-1Bi0.6Eu zinc calcium silicate glass samples.

3.3. Optical band gaps

Fig. 3 shows the direct optical band gaps (DOBG) (Fig. 3a) and indirect optical band gaps (IOBG) (Fig. 3b) of SZC-1.0Bi, SZC-0.6Eu, and SZC-1.0Bi0.6Eu zinc calcium silicate glass samples. DOBG and IOBG values for SZC-1.0Bi, SZC-0.6Eu, and SZC-1.0Bi0.6Eu zinc calcium silicate glass samples can be calculated based on the absorption spectra of these glass samples, and Tauc following formula:⁸

$$\alpha(\lambda) = A \cdot \frac{(h\nu - E_g)^\gamma}{h\nu} \quad (1)$$

In there, $\gamma = 1/2$ for the DOBG, and $\gamma = 2$ for the IOBG; E_g is the energy gap of SZC-1.0Bi, SZC-0.6Eu, and SZC-1.0Bi0.6Eu zinc calcium silicate glass samples; (λ) is the absorption coefficient; A is a proportionality constant; ν is the frequency; h is Planck's constant; λ is the wavelength. The relation between $\alpha(\lambda)$ and $h\nu$ is given by the Davis and Mott theory.³³ For each glass sample, (λ) is determined based on the expression:^{8,33}

$$\alpha(\lambda) = \frac{2.303}{d} \cdot E_{\text{opt}}(\lambda) \quad (2)$$

In there, $E_{\text{opt}}(\lambda)$ is the absorbance; d is the thickness of SZC zinc calcium silicate glass samples.³³

Thus, the DOBG values for SZC-1.0Bi, SZC-0.6Eu, and SZC-1.0Bi0.6Eu zinc calcium silicate glass samples were determined to be ~ 4.01 , 3.47, and 3.96 eV, respectively. Compared with the DOBG value of the SZC-0.6Eu zinc calcium silicate glass sample, the DOBG value of SZC-1.0Bi0.6Eu zinc calcium silicate glass sample was significantly greater with the energy difference $\Delta E_{\text{g(DOBG)}} = 3.96 \text{ eV} - 3.47 \text{ eV} = 0.49 \text{ eV}$. The IOBG values for SZC-1.0Bi, SZC-0.6Eu, and SZC-1.0Bi0.6Eu zinc calcium silicate glass samples were determined to be ~ 3.78 , 2.83, and 3.65 eV, respectively. Compared with the IOBG value of the SZC-0.6Eu zinc calcium silicate glass sample, the IOBG value of the SZC-1.0Bi0.6Eu zinc calcium silicate glass sample was also increased significantly with the energy difference $\Delta E_{\text{g(IOBG)}} = 3.65 \text{ eV} - 2.83 \text{ eV} = 0.82 \text{ eV}$. This result thus confirmed that both DOBG and IOBG values were significantly increased with the presence of Bi^{m+} ions in the SZC-1.0Bi0.6Eu zinc calcium silicate glass sample. On the contrary, when comparing the

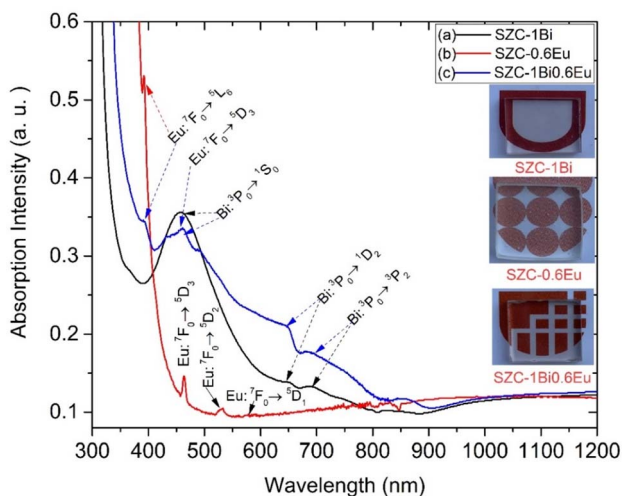


Fig. 2 Absorption spectra of SZC-1.0Bi, SZC-0.6Eu, and SZC-1.0Bi0.6Eu zinc calcium silicate glass samples.

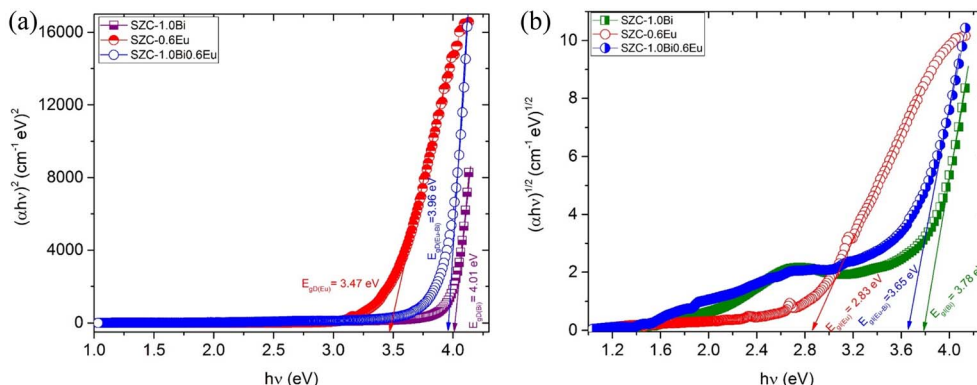


Fig. 3 (a) Direct optical band gaps of SZC-1.0Bi, SZC-0.6Eu, and SZC-1.0Bi0.6Eu zinc calcium silicate glass samples. (b) Indirect optical band gaps of SZC-1.0Bi, SZC-0.6Eu, and SZC-1.0Bi0.6Eu zinc calcium silicate glass samples.

DOBG and IOBG values of the SZC-1Bi sample with the corresponding DOBG and IOBG values of the SZC-1Bi0.6Eu sample, both DOBG and IOBG values of the SZC-1Bi0.6Eu sample are all significantly decreased. These results can be rationalized by the following reasons: (i) the absorption spectrum of the SZC-0.6Eu sample does not appear in the surface plasmon resonance (SPR),³⁴ whereas for the SZC-1Bi0.6Eu sample, the absorption spectrum appears in the SPR at the peak of ~ 458 nm of Bi^{m+} ions. Therefore, the $E_{\text{opt}}(\lambda)$ value of the SZC-1Bi0.6Eu sample increases more than the $E_{\text{opt}}(\lambda)$ value of the SZC-0.6Eu sample³⁴ leading to the values of both DOBG and IOBG of the sample SZC-1Bi0.6Eu increase according to formula (1); (ii) compared with the SZC-1Bi sample, the $E_{\text{opt}}(\lambda)$ value of the SZC-1Bi0.6Eu

sample decreases linearly in the presence of Eu^{n+} ions due to Eu^{n+} ions combining with Bi^{m+} ions to increase the non-bridging oxygen (NBO) bonds³⁵ leading to the band edge shift to higher energies.³⁵ The calculated results for DOBG and IOBG values in this work are also completely consistent with the results of previous studies^{36–39} and are compared in detail in Table 2. The IOBG value of SZC-1.0Bi, SZC-0.6Eu, and SZC-1.0Bi0.6Eu zinc calcium silicate glass samples showed that the green and blue curves exhibited shallow collisions centered about 2.71 eV. This result is due to both absorption spectra of SZC-1Bi and SZC-1Bi0.6Eu samples, the peak was at about 458 nm, corresponding to the $h\nu = 2.71$ eV, and thus it appeared the SPR attributed to Bi^{m+} ions.

3.4. Visible (VIS) emission

Visible (VIS) emission spectra of SZC-1.0Bi, SZC-0.6Eu, SZC-1.0Bi0.6Eu2Yb, and SZC-1.8Bi0.6Eu2Yb zinc calcium silicate glass samples under 320 nm excitation are shown in Fig. 4. For

Table 2 The comparison of direct and indirect optical band gaps in this work with previous related studies^{36–39}

Host materials	Doped/co-doped	DOBG (eV)	IOBG (eV)	Ref.
Germanium-borate glasses	1.0Bi ³⁺	—	3.43	X. Y. Liu <i>et al.</i> ³⁶
Germanium-borate glasses	1.0Bi ³⁺ /3.5Eu ³⁺	—	3.35	X. Y. Liu <i>et al.</i> ³⁶
Boron glasses	1Eu ³⁺	3.529	3.306	K. Maheshvaran <i>et al.</i> ³⁷
Boro-tellurite glasses	1Eu ³⁺	3.161	3.011	K. Maheshvaran <i>et al.</i> ³⁷
Zinc soda lime silica glasses	4.7Eu ³⁺	3.20	—	N. A. S. Omar <i>et al.</i> ³⁸
Borosilicate glasses	10Bi ³⁺ /0.6Eu ³⁺	3.430	3.419	D. V. K. Reddy <i>et al.</i> ³⁹
Borosilicate glasses	10Bi ³⁺ /1Eu ³⁺	3.456	3.449	D. V. K. Reddy <i>et al.</i> ³⁹
Zinc calcium silicate glasses	0.6Eu ³⁺	3.47	2.83	This study
Zinc calcium silicate glasses	1Bi ³⁺	4.01	3.78	This study
Zinc calcium silicate glasses	1Bi ³⁺ /0.6Eu ³⁺	3.96	3.65	This study

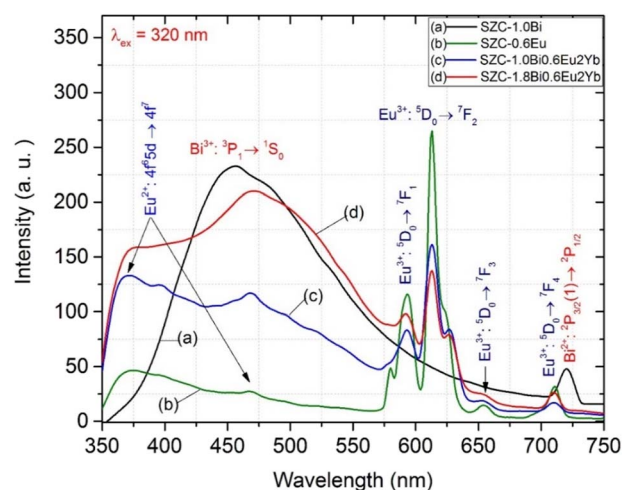


Fig. 4 VIS emission spectra of SZC-1.0Bi, SZC-0.6Eu, SZC-1.0Bi0.6Eu2Yb and SZC-1.8Bi0.6Eu2Yb zinc calcium silicate glass samples under 320 nm excitation.



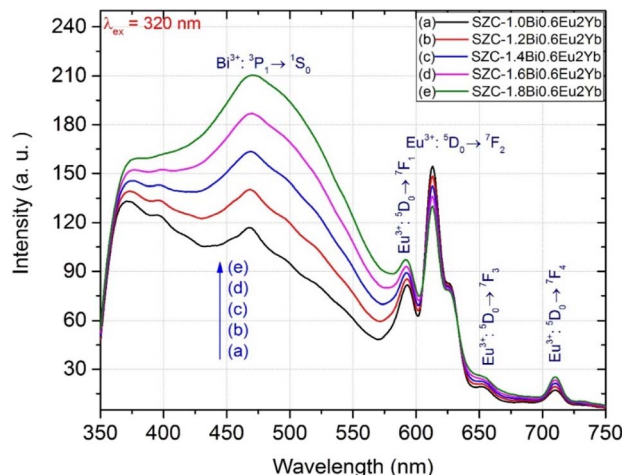


Fig. 5 VIS emission spectra of SZC-*x*Bi0.6Eu2Yb (*x* = 1.0, 1.2, 1.4, 1.6, and 1.8 mol%) zinc calcium silicate glass samples under 320 nm excitation.

the SZC-1.0Bi zinc calcium silicate glass sample, VIS emission spectra of Bi³⁺ ions were observed consisting of two peaks at ~457 and 720 nm, which are attributed to VIS emissions from ³P₁ → ¹S₀ transition of Bi³⁺ and ²P_{3/2}(1) → ²P_{1/2} transition of Bi²⁺,^{12,13} respectively. For the SZC-0.6Eu zinc calcium silicate glass sample, VIS emission spectra of Eu³⁺/Eu²⁺ ions were observed in a band from ~373 to 468 nm, attributed to VIS emission from 4f⁶5d¹ → 4f⁷ transition of Eu²⁺ ions,^{7,8} and four VIS emission peaks at ~593, 613, 654, and 710 nm attributed to ⁵D₀ → ⁷F_J (*J* = 1, 2, 3, and 4) transitions of Eu³⁺ ions.^{20,21} For the SZC-1.0Bi0.6Eu2Yb and SZC-1.8Bi0.6Eu2Yb zinc calcium silicate glass samples, VIS emission intensity of Eu³⁺/Eu²⁺ ions in the band of 373–468 nm was significantly increased due to ET process from Bi³⁺ to Eu²⁺ ions. The remaining VIS emission spectra of Eu³⁺ ions peaks at ~593, 613, 654, and 710 nm were also observed.^{21,22} However, the VIS emission spectra of Bi²⁺ ions peak at ~720 nm have ceased to exist and can not be observed. This result also means that the energy from the ²P_{3/2}(1) → ²P_{1/2} transition of Bi²⁺ ions is transferred to ⁵D₀ → ⁷F_J (*J* = 1, 2, 3, and 4) transitions of Eu³⁺ ions.^{20–22}

VIS emission spectra of SZC-*x*Bi0.6Eu2Yb (*x* = 1.0, 1.2, 1.4, 1.6, and 1.8 mol%) zinc calcium silicate glass samples under 320 nm excitation are shown in Fig. 5. With the increasing of Bi³⁺ concentrations from 1.0 up to 1.8 mol%, the VIS emission intensity of the peak at ~468 nm was strongly increased. At the same time, the VIS emission intensity of the peaks at ~593, 613, 654, and 710 nm of Eu³⁺ were also increased. This proves that the energy from ³P₁ → ¹S₀ transition of Bi³⁺ ions^{11,12} and ²P_{3/2}(1) → ²P_{1/2} transition of Bi²⁺ ions^{17,18} is transferred to ⁵D₀ → ⁷F_J (*J* = 1, 2, 3, and 4) transitions of Eu³⁺ ions.^{7,8,32}

For the Eu³⁺/Eu²⁺-doped and Bi³⁺/Eu³⁺/Eu²⁺ co-doped in the glass materials, the determination of color coordinates is significant for LED, WLED, and color display applications. Therefore, we calculated and determined CIE 1931 (*x*, *y*) color coordinates for these samples using the CIE chromaticity coordinates calculation software. CIE 1931 (*x*, *y*) color

coordinates for the VIS emission spectra of SZC-0.6Eu and SZC-*x*Bi0.6Eu2Yb (*x* = 1.0, 1.2, 1.4, 1.6, and 1.8 mol%) zinc calcium silicate glass samples under 320 nm excitation are described in detail in Fig. 6. For the Eu³⁺/Eu²⁺-doped in SZC-0.6Eu zinc calcium silicate glass sample, CIE 1931 (*x*, *y*) color coordinates for VIS emission were determined at P0 point in the pink region. For the Bi³⁺/Eu³⁺ co-doped in SZC-*x*Bi0.6Eu2Yb (*x* = 1.0, 1.2, 1.4, 1.6, and 1.8 mol%) zinc calcium silicate glass samples, CIE 1931 (*x*, *y*) color coordinates were determined at P1, P2, P3, P4, and P5 points in the white pink region, which is the neighborhood around black body curve. CIE 1931 (*x*, *y*) color coordinates of P0, P1, P2, P3, P4, and P5 points are listed in detail in Table 3.

3.5. Upconversion (UC) emission

Fig. 7 shows the UC emission spectra of SZC-1.8Bi_yEu2Yb (*y* = 0.6, 0.7, 0.8, 0.9, and 1.0 mol%) zinc calcium silicate glass samples under 980 nm LD excitation. From the results presented in Fig. 7, we can determine that the UC emission peaks at ~580, 593, 613, 654, and 706 nm, which are attributed to ⁵D₀ → ⁷F_J (*J* = 0, 1, 2, 3, and 4) transitions of Eu³⁺ ions.⁴⁰ Under 980 nm LD excitation, UC emission of Bi³⁺ ions was hardly observed at any peaks. At the same time, when increasing the Eu³⁺/Eu²⁺ concentrations from 0.6 up to 1.0 mol%, UC emission intensity of Eu³⁺ peaks at ~580, 593, 613, 654, and 706 nm was significantly increased.^{41,42} The mechanism of the UC process of Bi³⁺/Eu³⁺/Yb³⁺ co-doped is depicted in Fig. 10. When excited at the wavelength of 980 nm, two Yb³⁺ ions are formed Yb³⁺–Yb³⁺ pairs. Through the CET 1 process, the photons are transferred to the ⁵D₂ level of Eu³⁺. Then the photons rapidly transfer to the ⁵D₀ level via the non-radiative transition. The ⁵D₀ → ⁷F_J (*J* = 4, 3,

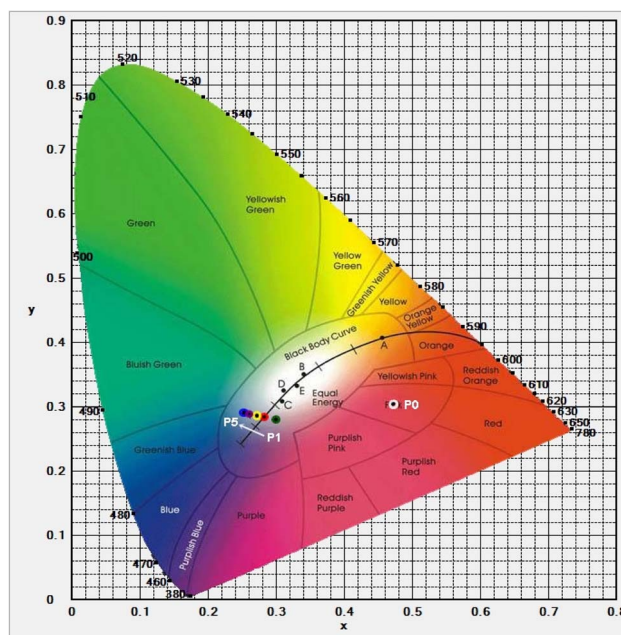


Fig. 6 CIE 1931 (*x*, *y*) color coordinates for VIS emission of SZC-0.6Eu and SZC-*x*Bi0.6Eu2Yb (*x* = 1.0, 1.2, 1.4, 1.6, and 1.8 mol%) zinc calcium silicate glass samples under 320 nm excitation.



Table 3 CIE 1931 (*x*, *y*) color coordinates of SZC-0.6Eu and SZC-*x*Bi0.6Eu2Yb (*x* = 1.0, 1.2, 1.4, 1.6, and 1.8 mol%) zinc calcium silicate glass samples under 320 nm excitation

Glass samples	Position on CIE 1931 chromaticity diagram	CIE 1931 (<i>x</i>)	CIE 1931 (<i>y</i>)
SZC-0.6Eu	P0	0.2534	0.2902
SZC-1.0Bi0.6Eu2Yb	P1	0.2992	0.2801
SZC-1.2Bi0.6Eu2Yb	P2	0.2832	0.2837
SZC-1.4Bi0.6Eu2Yb	P3	0.2710	0.2865
SZC-1.6Bi0.6Eu2Yb	P4	0.2614	0.2886
SZC-1.8Bi0.6Eu2Yb	P5	0.2537	0.2904

2, 1 and 0) transitions of Eu^{3+} produce the UC emissions peaks at ~580, 593, 613, 654, and 706 nm, respectively.

CIE 1931 (*x*, *y*) coordinates for the UC emission spectra of SZC-1.8Bi y Eu2Yb (*y* = 0.6, 0.7, 0.8, 0.9, and 1.0 mol%) zinc calcium silicate glass samples under 980 nm LD excitation is also described in detail in Fig. 8. Based on the results in Fig. 8, it can be seen that the CIE 1931 (*x*, *y*) color coordinates for UC emission spectra of SZC-1.8Bi y Eu2Yb (*y* = 0.6, 0.7, 0.8, 0.9 and 1.0 mol%) zinc calcium silicate glass samples were determined at M1, M2, M3, M4, and M5 points in the reddish-orange region. For the SZC-1.8Bi0.8Eu2Yb, SZC-1.8Bi0.9Eu2Yb, and SZC-1.8Bi1.0Eu2Yb zinc calcium silicate glass samples, although the UC emission intensity at ~580, 593, 613, 654, and 706 nm was significantly increased, but CIE 1931 (*x*, *y*) color coordinates changed very little, the M3, M4, and M5 points almost coincide. CIE 1931 (*x*, *y*) color coordinates of M1, M2, M3, M4, and M5 points are listed in detail in Table 4. Moreover, the comparison of the CIE 1931 (*x*, *y*) color coordinates in this study with those in a few previous related studies^{4,36,43–47} is presented in Table 5. From the results revealed in Table 5, we can confirm that with the difference of the host materials, the ratio of $\text{Bi}^{3+}/\text{Eu}^{3+}$ concentrations, and the excitation wavelength, the CIE 1931 (*x*, *y*) color coordinates also changes differently.

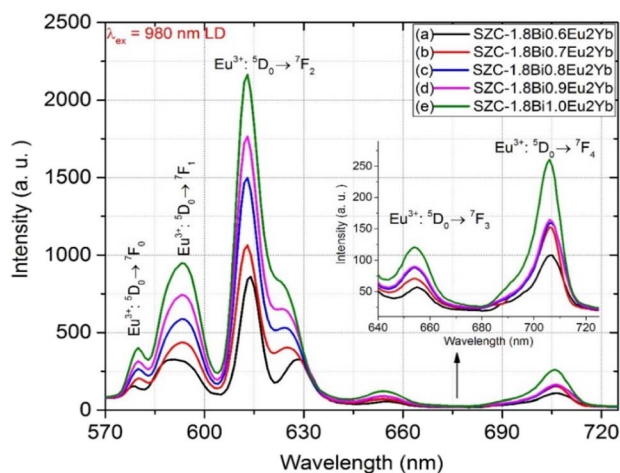


Fig. 7 UC emission spectra of SZC-1.8Bi y Eu2Yb (*y* = 0.6, 0.7, 0.8, 0.9, and 1.0 mol%) zinc calcium silicate glass samples.

3.6. NIR emission

NIR emission spectra of SZC-1Bi0.6Eu2Yb (*z* = 2.0, 2.2, 2.4, 2.6, and 2.8 mol%) zinc calcium silicate glass samples under excitation of 330 nm are shown in Fig. 9. It can be observed that the NIR emission spectra of $\text{Bi}^{m+}/\text{Eu}^{n+}/\text{Yb}^{3+}$ co-doped (*m* = 0, 2, 3 and *n* = 2, 3) consist of two emission peaks at ~986 and 1062 nm, which the NIR emission of $\text{Bi}^{m+}/\text{Eu}^{n+}/\text{Yb}^{3+}$ co-doped peak at ~986 nm due to $^2\text{F}_{5/2} \rightarrow ^2\text{F}_{7/2}$ transition of Yb^{3+} ions,⁴⁸ while the NIR emission peak at ~1062 nm can be attributed to $^2\text{D}_{3/2} \rightarrow ^4\text{S}_{3/2}$ transition of Bi^0 ions.^{48–50} In the NIR range of ~960–1040 nm, NIR emission spectra of $\text{Bi}^{m+}/\text{Eu}^{n+}/\text{Yb}^{3+}$ co-doped produced a bandwidth of ~40 nm. However, according to many previous reports, it has been attributed the NIR emission at ~1062 nm to Bi^0 ions because Bi-dopant exists at three states including Bi^{3+} , Bi^+ , and Bi^0 ions that can emit in NIR range from ~950 to 1500 nm.^{12,15–17} It thus has been confirmed that (i) NIR emission of Bi-doped peak around

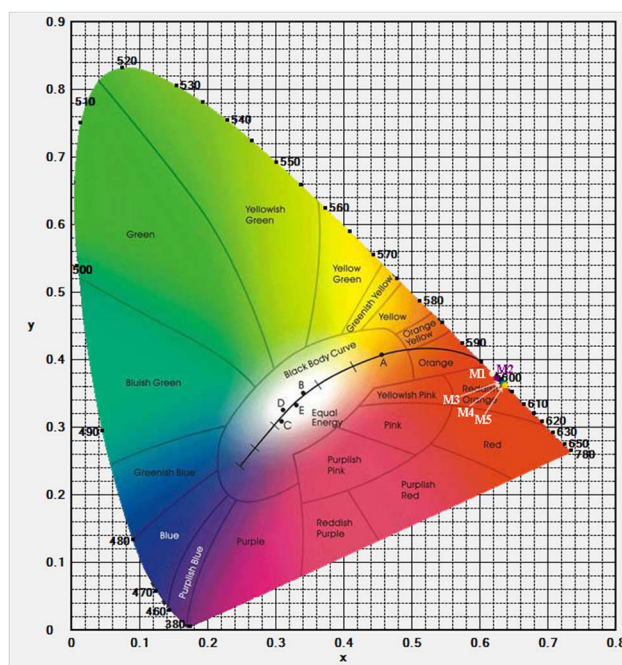


Fig. 8 CIE 1931 (*x*, *y*) for UC emission spectra of SZC-1.8Bi y Eu2Yb (*y* = 0.6, 0.7, 0.8, 0.9, and 1.0 mol%) zinc calcium silicate glass samples under 980 nm LD excitation.



Table 4 CIE 1931 (x, y) color coordinates of SZC-1.8Bi³⁺/Eu²⁺Yb (y = 0.6, 0.7, 0.8, 0.9, and 1.0 mol%) zinc calcium silicate glass samples under 980 nm LD excitation

Glass samples	Position on CIE 1931 chromaticity diagram	CIE 1931 (x)	CIE 1931 (y)
SZC-1.8Bi ³⁺ 0.6Eu ²⁺ Yb	M1	0.6239	0.3756
SZC-1.8Bi ³⁺ 0.7Eu ²⁺ Yb	M2	0.6293	0.3703
SZC-1.8Bi ³⁺ 0.8Eu ²⁺ Yb	M3	0.6317	0.3679
SZC-1.8Bi ³⁺ 0.9Eu ²⁺ Yb	M4	0.6321	0.3675
SZC-1.8Bi ³⁺ 1.0Eu ²⁺ Yb	M5	0.6322	0.3674

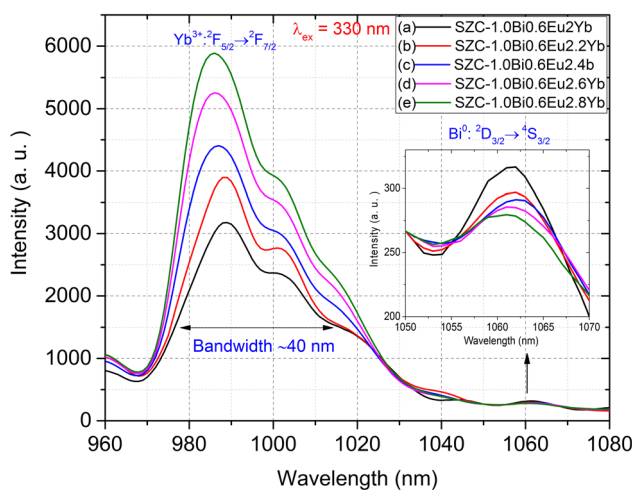
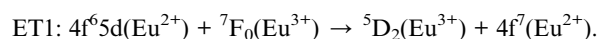
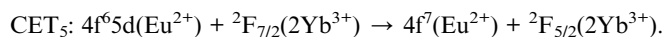
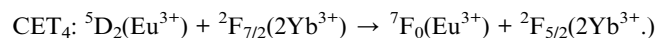
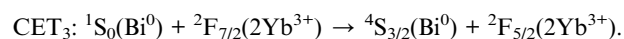
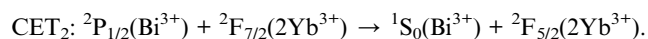
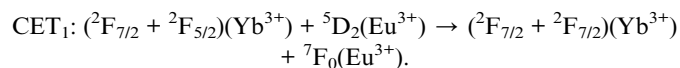
Table 5 The CIE 1931 (x, y) color coordinates in this work in comparison with those in previous related studies.^{4,36,43–47}

Host materials	Doped/co-doped	λ_{ex} (nm)	CIE 1931(x, y)	Color region	Ref.
Germanium-borate glasses	1.0Bi ³⁺ /0.5Eu ³⁺	345	(0.356, 0.325)	White	X. Y. Liu <i>et al.</i> ³⁶
Germanium-borate glasses	1.0Bi ³⁺ /3.5Eu ³⁺	345	(0.562, 0.371)	Reddish orange	X. Y. Liu <i>et al.</i> ³⁶
Ba ₂ Y ₅ B ₅ O ₁₇ phosphors	0.0005Bi ³⁺ /0.4Eu ³⁺	365	(0.415, 0.359)	Orange pink	G. Annadurai <i>et al.</i> ⁴³
Lu ₂ Ge ₂ O ₇ phosphors	0.06Bi ³⁺ /0.2Eu ³⁺	290	(0.558, 0.232)	Purplish red	Q. F. Li <i>et al.</i> ⁴
(Ba, Sr) ₃ Sc ₄ O ₉ solid solution compounds	0.03Bi ³⁺ /0.3Eu ³⁺	330	(0.575, 0.340)	Reddish orange	P. P. Dang <i>et al.</i> ⁴⁴
Silicate glasses	2Bi ³⁺ /0.3Eu ³⁺	333	(0.595, 0.352)	Reddish orange	O. G. Giraldo <i>et al.</i> ⁴⁵
KY ₃ F ₁₀ oxyfluoride glass-ceramics	0.3Bi ³⁺ /0.4Eu ³⁺	280	(0.2969, 0.2275)	Reddish purple	B. C. Yu <i>et al.</i> ⁴⁶
LaNbO ₄ phosphor	0.12Eu ³⁺ /0.05Yb ³⁺	980	(0.560, 0.390)	Orange	A. Dwivedi <i>et al.</i> ⁴⁷
Zinc calcium silicate glasses	0.6Eu ³⁺	320	(0.2534, 0.2902)	Pink	This study
Zinc calcium silicate glasses	1Bi ³⁺ /0.6Eu ³⁺ /2Yb ³⁺	320	(0.2992, 0.2801)	Purplish blue (near the white area)	This study
Zinc calcium silicate glasses	1.8Bi ³⁺ /0.6Eu ³⁺ /2Yb ³⁺	980	(0.6239, 0.3756)	Reddish orange	This study

1100 nm was attributed to Bi⁰ ions;³⁸ (ii) the NIR emission spectrum of Bi³⁺ ions was unobserved in the NIR wavelength range^{15–17} and that NIR emission of Bi³⁺ under different excitation wavelengths is usually emitted from ~1250 to 1500 nm.^{11,39} With the increase of Yb³⁺ concentrations from 2.0 up to

2.8 mol% and Bi^{m+} concentrations remained unchanged, NIR emission intensity of Bi⁰ ions peak at ~1062 nm was decreased. This result has confirmed that ET from ²D_{3/2} → ⁴S_{3/2} transition of Bi⁰ ions to ²F_{5/2} → ²F_{7/2} transition of Yb³⁺ ions has occurred. At the same time, the NIR emission intensity of Bi^{m+}/Euⁿ⁺/Yb³⁺ co-doped peak at ~986 nm was strongly increased due to the energy contribution of cooperative ET (CET)₄ and CET₅ processes from Eu³⁺ and Eu²⁺ ions to Yb³⁺ ions.^{40,41}

Mechanism of CET_I (I from 1 to 5) and ET_J (J from 1 to 4) processes among Euⁿ⁺, Bi^{m+}, and Yb³⁺ ions in SZC zinc calcium silicate glasses are described and defined in detail in Fig. 10. CET_I (I from 1 to 5) and ET_J (J from 1 to 4) processes were described as follows:^{50–52}

**Fig. 9** NIR emission spectra of SZC-1.8Bi^{0.6}Eu²Yb (z = 2.0, 2.2, 2.4, 2.6, and 2.8 mol%) zinc calcium silicate glass samples.

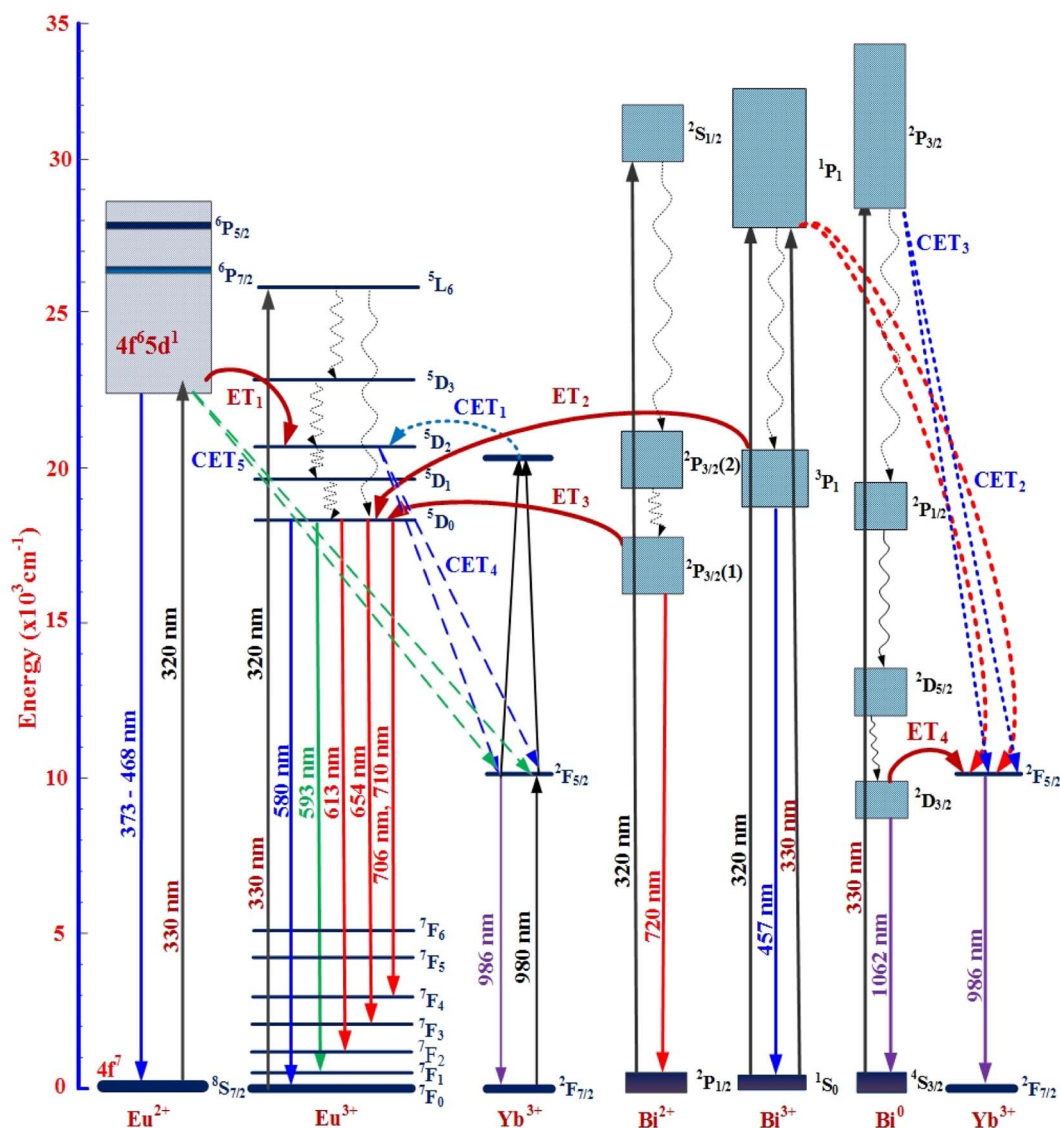
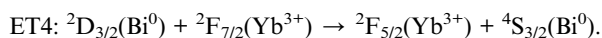
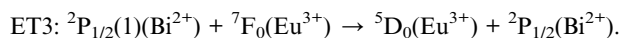
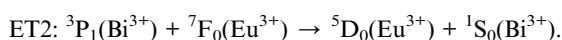


Fig. 10 Energy levels, VIS-, UC-, NIR-emissions and mechanism of CET_{*l*} (*l* from 1 to 5), and ET_{*J*} (*J* from 1 to 4) processes between Bi^{*m*+}, Eu^{*n*+}, and Yb³⁺ in SZC zinc calcium silicate glasses.



4. Conclusions

In this work, we have successfully synthesized zinc calcium silicate glass with the main compositions of SiO₂-ZnO-CaF₂-LaF₃-TiO₂-Bi₂O₃-EuF₃-YbF₃. The DOBG and IOBG values for Bi^{*m*+}/Eu^{*n*+} co-doped in SZC-1.0Bi0.6Eu zinc calcium silicate glass samples were determined at ~3.65 and 3.96 eV, respectively. Both of these values were increased in the presence of

Bi^{*m*+} ions in SZC-1.0Bi0.6Eu zinc calcium silicate glass samples. Under the excitation of 320 nm, VIS emission spectra of Bi^{*m*+}/Eu^{*n*+}/Yb³⁺ co-doped were observed in the peaks at ~468, 593, 613, 654, and 710 nm attributed to Bi³⁺, Bi²⁺, Eu³⁺, and Eu²⁺ ions. CIE 1931 (*x*, *y*) color coordinates for VIS emission spectra of Bi^{*m*+}/Eu^{*n*+}/Yb³⁺ co-doped zinc calcium silicate glass samples were determined in the white-pink region neighborhood around the black body curve. UC emission spectra of Bi^{*m*+}/Eu^{*n*+}/Yb³⁺ co-doped were observed in the peaks at ~580, 593, 613, 654, and 706 nm attributed to Eu²⁺ ions. CIE 1931 (*x*, *y*) color coordinates for UC emission spectra of Bi^{*m*+}/Eu^{*n*+}/Yb³⁺ co-doped zinc calcium silicate glass samples were determined in the reddish-orange region. NIR emission spectra of Bi^{*m*+}/Eu^{*n*+}/Yb³⁺ co-doped have two emission peaks at ~986 and 1062 nm, attributed to Yb³⁺ and Bi⁰ ions, respectively. NIR emission

spectra of $\text{Bi}^{m+}/\text{Eu}^{n+}/\text{Yb}^{3+}$ co-doped produced a bandwidth of ~ 40 nm in the wavelength range of ~ 960 to 1040 nm. The energy from $^3\text{P}_1 \rightarrow ^1\text{S}_0$ transition of Bi^{3+} ions and $^2\text{P}_{3/2}(1) \rightarrow ^2\text{P}_{1/2}$ transition of Bi^{2+} ions transferred to $^5\text{D}_0 \rightarrow ^7\text{F}_J$ ($J=1, 2, 3$, and 4) transitions of Eu^{3+} ions and ET process from $^2\text{D}_{3/2} \rightarrow ^4\text{S}_{3/2}$ transition of Bi^0 ions to $^2\text{F}_{5/2} \rightarrow ^2\text{F}_{7/2}$ transition of Yb^{3+} ions also occurred. The $\text{Bi}^{m+}/\text{Eu}^{n+}/\text{Yb}^{3+}$ co-doped zinc calcium silicate glasses in this study can be further developed for LED, WLED, display, and solar cell applications.

Conflicts of interest

There are no conflicts to declare.

Acknowledgements

This research is funded by Projects B2022-TNA-37 of the Vietnam Ministry of Education and Training. The author Ho Kim Dan would like to express his gratitude to Van Lang University.

References

- 1 A. D. Sontakke, A. J. van Bunningen, F. T. Rabouw, S. Meijers and A. Meijerink, Unraveling the $\text{Eu}^{2+} \rightarrow \text{Mn}^{2+}$ energy transfer mechanism in W-LED phosphors, *J. Phys. Chem. C*, 2020, **124**(25), 13902–13911, DOI: [10.1021/acs.jpcc.0c03425](https://doi.org/10.1021/acs.jpcc.0c03425).
- 2 H. K. Dan, D. C. Zhou, R. F. Wang, Q. Jiao, Z. W. Yang, Z. G. Song, X. Yu and J. B. Qiu, Effect of Mn^{2+} ions on the enhancement red upconversion emission and energy transfer of $\text{Mn}^{2+}/\text{Tm}^{3+}/\text{Yb}^{3+}$ tri-doped transparent glass-ceramics, *Mater. Res. Bull.*, 2016, **73**, 357–361, DOI: [10.1016/j.materresbull.2015.09.019](https://doi.org/10.1016/j.materresbull.2015.09.019).
- 3 X. Yu, L. Zhang, X. H. Xu, T. Wang, H. L. Yu, T. M. Jiang, Q. Jiao, Z. W. Yang, D. C. Zhou and J. B. Qiu, Development of a single-phased $\text{Ca}_3\text{SnSi}_2\text{O}_9$: Bi^{3+} , Dy^{3+} , Eu^{3+} phosphor with tri-colors for white light-emitting diodes, *J. Lumin.*, 2014, **145**, 114–118, DOI: [10.1016/j.jlumin.2013.07.009](https://doi.org/10.1016/j.jlumin.2013.07.009).
- 4 Q. F. Li, S. A. Zhang, W. X. Lin, W. F. Li, Y. X. Li, Z. F. Mu and F. G. Wu, A warm white emission of Bi^{3+} - Eu^{3+} and Bi^{3+} - Sm^{3+} codoping $\text{Lu}_2\text{Ge}_2\text{O}_7$ phosphors by energy transfer of Bi^{3+} -sensitized $\text{Eu}^{3+}/\text{Sm}^{3+}$, *Spectrochim. Acta, Part A*, 2020, **228**(5), 117755, DOI: [10.1016/j.saa.2019.117755](https://doi.org/10.1016/j.saa.2019.117755).
- 5 Y. Zhydachevskyy, I. I. Syvorotkac, V. Tsiurmaa, M. Barand, L. Lipińskad, A. Wierzbickaa and A. Suchocki, Quantum efficiency of the down-conversion process in Bi^{3+} - Yb^{3+} and Ce^{3+} - Yb^{3+} co-doped garnets, *Sol. Energy Mater. Sol. Cells*, 2018, **185**, 240–251, DOI: [10.1016/j.solmat.2018.05.037](https://doi.org/10.1016/j.solmat.2018.05.037).
- 6 X. Liu, C. Chen, S. Li, Y. Dai, H. Guo, X. Tang, Y. Xie and L. Yan, Host-sensitized and tunable luminescence of $\text{GdNbO}_4\text{:Ln}^{3+}$ ($\text{Ln}^{3+} = \text{Eu}^{3+}/\text{Tb}^{3+}/\text{Tm}^{3+}$) nanocrystalline phosphors with abundant color, *Inorg. Chem.*, 2016, **55**, 10383–10396, DOI: [10.1021/acs.inorgchem.6b01637](https://doi.org/10.1021/acs.inorgchem.6b01637).
- 7 Y. D. Ma, M. Z. Fei, W. N. Zhang, L. M. Teng, F. F. Hu, R. F. Wei and H. Guo, Energy transfer and tunable luminescent properties in $\text{Eu}^{2+}/\text{Tb}^{3+}/\text{Eu}^{3+}$ co-doped oxyfluoride aluminosilicate glass, *J. Lumin.*, 2020, **219**, 116966, DOI: [10.1016/j.jlumin.2019.116966](https://doi.org/10.1016/j.jlumin.2019.116966).
- 8 H. K. Dan, N. D. Trung, T. H. Le, N. L. Thai, N. M. Ty, D. C. Zhou and J. B. Qiu, Influence of F^- on the reduction process of Eu^{3+} to Eu^{2+} and optical properties of $\text{Eu}^{3+}/\text{Eu}^{2+}$ - Er^{3+} - Yb^{3+} co-doped niobate silicate glasses, *J. Non-Cryst. Solids*, 2022, **581**, 121417, DOI: [10.1016/j.jnoncrystol.2022.121417](https://doi.org/10.1016/j.jnoncrystol.2022.121417).
- 9 W. P. Chen, Y. J. Ouyang, M. Mo, H. Z. Zhang and Q. Su, Observation of energy transfer from Eu^{2+} to Eu^{3+} and tunable luminescence in phosphors $\text{YF}_3\text{:Eu}$ prepared by hydrothermal method, *J. Lumin.*, 2021, **229**, 117672, DOI: [10.1016/j.jlumin.2020.117672](https://doi.org/10.1016/j.jlumin.2020.117672).
- 10 H. Bouchouicha, G. Panczer, D. de Ligny, Y. Guyot, M. L. Baesso, L. H. C. Andrade, S. M. Lima and R. Ternane, Synthesis and luminescent properties of $\text{Eu}^{3+}/\text{Eu}^{2+}$ co-doped calcium aluminosilicate glass - ceramics, *J. Lumin.*, 2016, **169**, 528–533, DOI: [10.1016/j.jlumin.2014.11.054](https://doi.org/10.1016/j.jlumin.2014.11.054).
- 11 Q. S. Wu, Y. Y. Li, Y. J. Wang, H. Liu, S. S. Ye, L. Zhao, J. Y. Ding and J. C. Zhou, A novel narrow-band blue-emitting phosphor of Bi^{3+} -activated $\text{Sr}_3\text{Lu}_2\text{Ge}_3\text{O}_{12}$ based on a highly symmetrical crystal structure used for WLEDs and FEDs, *Chem. Eng. J.*, 2020, **401**, 126130, DOI: [10.1016/j.cej.2020.126130](https://doi.org/10.1016/j.cej.2020.126130), <https://www.sciencedirect.com/journal/chemical-engineering-journal/vol/401/suppl/C1>.
- 12 M. Puchalska, P. Bolek, K. Kot and E. Zych, Luminescence of Bi^{3+} and Bi^{2+} ions in novel Bi-doped SrAl_4O_7 phosphor, *Opt. Mater.*, 2020, **107**, 109999, DOI: [10.1016/j.optmat.2020.109999](https://doi.org/10.1016/j.optmat.2020.109999).
- 13 R. P. Cao, M. Y. Peng and J. R. Qiu, Photoluminescence of Bi^{2+} -doped BaSO_4 as a red phosphor for white LEDs, *Opt. Express*, 2012, **20**(S6), A977–A983, DOI: [10.1364/OE.20.00A977](https://doi.org/10.1364/OE.20.00A977).
- 14 N. Zhang, K. N. Sharafudeen, G. P. Dong, M. Y. Peng and J. R. Qiu, Mixed network effect of broadband near-infrared emission in Bi-Doped B_2O_3 - GeO_2 glasses, *J. Am. Ceram. Soc.*, 2012, **95**(12), 3842–3846, DOI: [10.1111/jace.12016](https://doi.org/10.1111/jace.12016).
- 15 R. F. Wang, J. Liu and Z. Zhang, Luminescence and energy transfer progress in Bi-Yb co-doped germanate glass, *J. Alloys Compd.*, 2016, **688**, 332–336, DOI: [10.1016/j.jallcom.2016.07.152](https://doi.org/10.1016/j.jallcom.2016.07.152).
- 16 Y. P. Tai, B. L. Pan, X. G. Du, H. Y. Liu, R. Q. Niu and X. Z. Li, Broadband downconversion in Bi^{3+} - Yb^{3+} -codoped transparent glass ceramics containing LaF_3 nanocrystals, *J. Mater. Sci.: Mater. Electron.*, 2020, **31**, 5117–5123, DOI: [10.1007/s10854-020-03072-9](https://doi.org/10.1007/s10854-020-03072-9).
- 17 A. J. Huang, Z. W. Yang, C. Y. Yu, Z. Z. Chai, J. B. Qiu and Z. G. Song, Near-infrared quantum cutting luminescence and energy transfer mechanism of $\text{Ba}_2\text{Y}(\text{BO}_3)_2\text{Cl}$: Bi^{3+} , Yb^{3+} phosphors, *IEEE Photonics J.*, 2018, **10**, 8400307, DOI: [10.1109/JPHOT.2017.2782842](https://doi.org/10.1109/JPHOT.2017.2782842).
- 18 L.-T. Lin, J.-Q. Chen, C. Deng, L. Tang, D.-J. Chen, J.-X. Meng and L.-W. Cao, Broadband near-infrared quantum-cutting by cooperative energy transfer in Yb^{3+} - Bi^{3+} co-doped CaTiO_3 for solar cells, *J. Alloys Compd.*, 2015, **640**, 280–284, DOI: [10.1016/j.jallcom.2015.04.031](https://doi.org/10.1016/j.jallcom.2015.04.031).
- 19 E. Lee, R. E. Kroon, J. J. Terblans and H. C. Swart, Luminescence properties of Y_2O_3 : Bi^{3+} , Yb^{3+} co-doped



- phosphor for application in solar cells, *Phys. B*, 2018, **535**(15), 102–105, DOI: [10.1016/j.physb.2017.06.072](https://doi.org/10.1016/j.physb.2017.06.072).
- 20 R. P. Cao, Z. Y. Huang, B. Lan, L. Li, X. H. Yi, Z. Y. Luo, C. X. Liao and J. Wang, Adjustable luminescence properties of Eu^{3+} and Bi^{3+} codoped $\text{Ca}_3\text{Zn}_3\text{Te}_2\text{O}_{12}$ phosphor, *Mater. Res. Bull.*, 2022, **152**, 111851, DOI: [10.1016/j.materresbull.2022.111851](https://doi.org/10.1016/j.materresbull.2022.111851), <https://www.sciencedirect.com/journal/materials-research-bulletin/vol/152/suppl/C>.
 - 21 H. Zhang, M. S. Liao, Y. Jiao, W. C. Li, H. H. Dong, Y. Z. Fang, W. Q. Gao and L. L. Hu, Color-tunable emissions in $\text{Bi}^{3+}/\text{Eu}^{3+}$ activated phosphors for multi-mode optical thermometers, *Ceram. Interfaces*, 2022, **48**(22), 33072–33081, DOI: [10.1016/j.ceramint.2022.07.240](https://doi.org/10.1016/j.ceramint.2022.07.240), <https://www.sciencedirect.com/journal/ceramics-international/vol/48/issue/22>.
 - 22 L. D. Guo, T. Li, C. C. Zhu, W. C. Liang and L. N. Wu, Tunable luminescent chromaticity of $\text{CaZnOS: Bi}^{3+}, \text{Eu}^{3+}$ with white emitting based on energy transfer, *J. Alloys Compd.*, 2022, **905**, 164262, DOI: [10.1016/j.jallcom.2022.164262](https://doi.org/10.1016/j.jallcom.2022.164262).
 - 23 Z. Tang, J. Q. Qi, Z. Y. Huang, L. X. Liang, A. J. Liu, Y. C. Ye, Y. T. Zhang and T. C. Lu, Novel multicolor-tunable $\text{Eu}^{3+}/\text{Bi}^{3+}$ co-doped $\text{Y}_2\text{Zr}_2\text{O}_7$ transparent ceramics as potential white-light-emitting materials, *Ceram. Interfaces*, 2022, **48**(3), 4216–4222, DOI: [10.1016/j.ceramint.2021.10.213](https://doi.org/10.1016/j.ceramint.2021.10.213), <https://www.sciencedirect.com/journal/ceramics-international/vol/48/issue/22>.
 - 24 E. Erol, N. Vahedigharehchopogh, O. Kibrıslı, M. C. Ersundu and A. E. Ersundu, Recent progress in lanthanide-doped luminescent glasses for solid-state lighting applications - a review, *J. Phys.: Condens. Matter*, 2021, **33**, 483001, DOI: [10.1088/1361-648X/ac22d9](https://doi.org/10.1088/1361-648X/ac22d9).
 - 25 H. K. Dan, N. M. Ty, D. C. Zhou, J. B. Qiu and A.-L. Phan, Influence of Cr^{3+} on yellowish-green UC emission and energy transfer of $\text{Er}^{3+}/\text{Cr}^{3+}/\text{Yb}^{3+}$ tri-doped zinc silicate glasses, *J. Am. Ceram. Soc.*, 2020, **103**(11), 1–13, DOI: [10.1111/jace.17359](https://doi.org/10.1111/jace.17359).
 - 26 D. Ehrt and S. Flügel, Properties of zinc silicate glasses and melts, *J. Mater. Sci. Eng.*, 2011, **A 1**, 312–320.
 - 27 H. K. Dan, D. C. Zhou, R. F. Wang, Q. Jiao, Z. W. Yang, Z. G. Song, X. Yu and J. B. Qiu, Effect of Mn^{2+} ions on the enhancement upconversion emission and energy transfer of $\text{Mn}^{2+}/\text{Tb}^{3+}/\text{Yb}^{3+}$ tri-doped transparent glass-ceramics, *Mater. Lett.*, 2015, **150**, 76–80, DOI: [10.1016/j.matlet.2015.03.005](https://doi.org/10.1016/j.matlet.2015.03.005).
 - 28 H. K. Dan, A.-L. Phan, N. M. Ty, D. C. Zhou and J. B. Qiu, Optical bandgaps and visible/near-infrared emissions of Bi^{3+} -doped ($n = 1, 2$, and 3) fluoroaluminosilicate glasses via Ag^+-K^+ ions exchange process, *Opt. Mater.*, 2021, **112**, 110762, DOI: [10.1016/j.optmat.2020.110762](https://doi.org/10.1016/j.optmat.2020.110762).
 - 29 H. K. Dan, T. D. Tap, H. Nguyen-Truong, N. M. Ty, D. C. Zhou and J. B. Qiu, Effects of heat treatment and Yb^{3+} concentration on the downconversion emission of $\text{Er}^{3+}/\text{Yb}^{3+}$ co-doped transparent silicate glass-ceramics, *Mater. Res.*, 2019, **22**(5), e20190113, DOI: [10.1590/1980-5373-MR-2019-0113](https://doi.org/10.1590/1980-5373-MR-2019-0113).
 - 30 Y. G. Liao, *X-Ray emission lines & Periodic table for EDS Analysis, Practical Electron Microscopy and Database - An Online Book*, <https://www.globalsino.com/EM>, accessed 15 November 2022.
 - 31 N. W. M. Ritchie, D. E. Newbury, H. Lowers and M. Mengason, Exploring the limits of EDS microanalysis: rare earth element analyses, *IOP Conf. Ser.: Mater. Sci. Eng.*, 2018, **304**, 012013, DOI: [10.1088/1757-899X/304/1/012013](https://doi.org/10.1088/1757-899X/304/1/012013).
 - 32 K. Lenczewska, Y. Gerasymchuk, N. Vu, N. Q. Liem, G. Boulon and D. Hreniak, The size effect on the energy transfer in $\text{Bi}^{3+}-\text{Eu}^{3+}$ co-doped GdVO_4 nanocrystals, *J. Mater. Chem. C*, 2017, **5**, 3014–3023, DOI: [10.1039/C6TC04660F](https://doi.org/10.1039/C6TC04660F).
 - 33 N. F. Mott and E. A. Davis, *Electronic processes in Non-crystalline materials*, Oxford, UK, Clarendon, 2nd edn, 1979.
 - 34 S. P. Singh and B. Karmakar, Photoluminescence enhancement of Eu^{3+} by energy transfer from Bi^{2+} to Eu^{3+} in bismuth glass nanocomposites, *RSC Adv.*, 2011, **1**, 751–754, DOI: [10.1039/C1RA00160D](https://doi.org/10.1039/C1RA00160D).
 - 35 M. H. M. Zaid, K. A. Matori, S. H. A. Aziz, A. Zakaria and M. S. M. Ghazali, Effect of ZnO on the physical properties and optical band gap of soda lime silicate glass, *Int. J. Mol. Sci.*, 2012, **13**, 7550–7558, DOI: [10.3390/ijms13067550](https://doi.org/10.3390/ijms13067550).
 - 36 X. Y. Liu, H. Guo, S. X. Dai, M. Y. Peng and Q. Y. Zhang, Energy transfer and thermal stability in $\text{Bi}^{3+}/\text{Eu}^{3+}$ co-doped germanium-borate glasses for organic-resin-free UV LEDs, *Opt. Mater. Express*, 2016, **6**(11), 3574, DOI: [10.1364/OME.6.003574](https://doi.org/10.1364/OME.6.003574).
 - 37 K. Maheshvaran, P. K. Veeran and K. Marimuthu, Structural and optical studies on Eu^{3+} doped boro-tellurite glasses, *Solid State Sci.*, 2013, **17**, 54–62, DOI: [10.1016/j.solidstatesciences.2012.11.013](https://doi.org/10.1016/j.solidstatesciences.2012.11.013).
 - 38 N. A. S. Omar, Y. W. Fen, K. A. Matori, M. H. M. Zaid and N. F. Samsudin, Structural and optical properties of Eu^{3+} activated low cost zinc soda lime silica glasses, *Results Phys.*, 2016, **6**, 640–644, DOI: [10.1016/j.rinp.2016.09.007](https://doi.org/10.1016/j.rinp.2016.09.007).
 - 39 D. V. K. Reddy, S. Taherunnisa, A. L. Prasanna, T. S. Rao, N. Veeraiah and M. R. Reddy, Enhancement of the red emission of Eu^{3+} by Bi^{3+} sensitizers in yttrium alumino bismuth borosilicate glasses, *J. Mol. Struct.*, 2019, **1176**(15), 133–148, DOI: [10.1016/j.molstruc.2018.08.057](https://doi.org/10.1016/j.molstruc.2018.08.057).
 - 40 A. Dwivedi, K. Mishra and S. B. Rai, Investigation of upconversion, downshifting and quantum-cutting behavior of Eu^{3+} , Yb^{3+} , Bi^{3+} co-doped LaNbO_4 phosphor as a spectral conversion material, *Methods Appl. Fluoresc.*, 2018, **6**, 035001, DOI: [10.1088/2050-6120/aab253](https://doi.org/10.1088/2050-6120/aab253).
 - 41 X. X. Han, E. H. Song, W. B. Chen, Y. Y. Zhou and Q. Y. Zhang, Color-tunable upconversion luminescence and prolonged Eu^{3+} fluorescence lifetime in fluoride $\text{KCaF}_3:\text{Yb}^{3+}, \text{Mn}^{2+}, \text{Eu}^{3+}$ via controllable and efficient energy transfer, *J. Mater. Chem. C*, 2020, **8**, 9836–9844, DOI: [10.1039/D0TC01502D](https://doi.org/10.1039/D0TC01502D).
 - 42 J. F. Li, Y. Long, Q. C. Zhao, S. P. Zheng, Z. J. Fang and B.-U. Guan, Efficient white upconversion luminescence in $\text{Yb}^{3+}/\text{Eu}^{3+}$ doubly-doped transparent glass ceramic, *Opt. Express*, 2021, **29**(14), 21763, DOI: [10.1364/OE.431959](https://doi.org/10.1364/OE.431959).
 - 43 G. Annadurai, L. L. Sun, H. Guo and X. Y. Huang, Bright tunable white-light emissions from $\text{Bi}^{3+}/\text{Eu}^{3+}$ co-doped $\text{Ba}_2\text{Y}_5\text{B}_5\text{O}_{17}$ phosphors via energy transfer for UV-excited



- white light-emitting diodes, *J. Lumin.*, 2020, **226**, 117474, DOI: [10.1016/j.jlumin.2020.117474](https://doi.org/10.1016/j.jlumin.2020.117474).
- 44 P. P. Dang, S. S. Liang, G. G. Li, H. Z. Lian, M. M. Shang and J. Lin, Broad color tuning of Bi³⁺/Eu³⁺-doped (Ba, Sr)₃Sc₄O₉ solid solution compounds *via* crystal field modulation and energy transfer, *J. Mater. Chem. C*, 2018, **6**, 9990, DOI: [10.1039/C8TC03334J](https://doi.org/10.1039/C8TC03334J).
- 45 O. G. Giraldo, M. Z. Fei, R. F. Wei, L. M. Teng, Z. G. Zheng and H. Guo, Energy transfer and white luminescence in Bi³⁺/Eu³⁺ co-doped oxide glasses, *J. Lumin.*, 2020, **219**, 116918, DOI: [10.1016/j.jlumin.2019.116918](https://doi.org/10.1016/j.jlumin.2019.116918).
- 46 B. C. Yu, X. Zhou, H. P. Xia, B. J. Chen and H. W. Song, Novel Bi³⁺/Eu³⁺ co-doped oxyfluoride transparent KY₃F₁₀ glass ceramics with wide tunable emission and high optical temperature sensitivity, *J. Lumin.*, 2021, **239**, 118366, DOI: [10.1016/j.jlumin.2021.118366](https://doi.org/10.1016/j.jlumin.2021.118366).
- 47 A. Dwivedi, K. Mishra and S. B. Rai, Investigation of Upconversion, downshifting and quantum -cutting behavior of Eu³⁺, Yb³⁺, Bi³⁺ co-doped LaNbO₄ phosphor as a spectral conversion material, *Methods Appl. Fluoresc.*, 2018, **6**, 035001, DOI: [10.1088/2050-6120/aab253](https://doi.org/10.1088/2050-6120/aab253).
- 48 M. Peng, B. Sprenger, M. A. Schmidt, H. G. L. Schwefel and L. Wondraczek, Broadband NIR photoluminescence from Bi-doped Ba₂P₂O₇ crystals: Insights into the nature of NIR-emitting Bismuth centers, *Opt. Express*, 2010, **18**, 12852–12863, DOI: [10.1364/OE.18.012852](https://doi.org/10.1364/OE.18.012852).
- 49 J. D. Wu, D. P. Chen, X. K. Wu and J. R. Qiu, Ultra-broad near-infrared emission of Bi-doped SiO₂-Al₂O₃-GeO₂ optical fibers, *Chine, Opt. Lett.*, 2011, **9**(7), 071601, DOI: [10.3788/COL201109.071601](https://doi.org/10.3788/COL201109.071601).
- 50 F. G. Chen, Y. F. Wang, W. W. Chen, P. X. Xiong, B. F. Jiang, S. F. Zhou, Z. J. Ma and M. Y. Peng, Regulating the Bi NIR luminescence behaviours in fluorine and nitrogen co-doped germanate glasses, *Mater. Adv.*, 2021, **2**, 4743–4751, DOI: [10.1039/D1MA00395J](https://doi.org/10.1039/D1MA00395J).
- 51 M.-H. Qu, R.-Z. Wang, Y. Zhang, K.-Y. Li and H. Yan, High efficient antireflective down-conversion Y₂O₃: Bi, Yb films with pyramid preferred oriented nano-structure, *J. Appl. Phys.*, 2012, **111**, 093108, DOI: [10.1063/1.4712461](https://doi.org/10.1063/1.4712461).
- 52 Y. P. Tai, G. J. Zheng, H. Wang and J. T. Bai, Broadband down-conversion based near-infrared quantum cutting in Eu²⁺-Yb³⁺ co-doped SrAl₂O₄ for crystalline silicon solar cells, *J. Solid State Chem.*, 2015, **226**, 250–254, DOI: [10.1016/j.jssc.2015.02.020](https://doi.org/10.1016/j.jssc.2015.02.020).

